Arabian Journal of Geosciences (2023) 16:487
https://doi.org/10.1007/s12517-023-11599-4

ORIGINAL PAPER

Major and trace element geochemistry of the Atrai River sediments from the Bengal Basin (Bangladesh): implication for provenance, chemical weathering, and tectonic setting in the southeastern Himalaya

Abu Sadat Md. Sayem[1] · Md. Rokonuzzaman[1] · Md. Shams Shahriar[2] · Rashed Abdullah[1] · Zahidul Bari[1] · Md. Sazzad Hossen[1]

Received: 31 March 2023 / Accepted: 13 July 2023 / Published online: 24 July 2023

Abstract
The Atrai River rises in the southeast Himalaya and empties into the Bengal Basin in the northwest. In this study, major and trace element geochemistry of the Atrai River sediments is carried out in addition to petrography to determine the compositional maturity, provenance, chemical weathering, and tectonic setting. X-ray fluorescence (XRF) spectrometry was employed for geochemical studies. Results reveal that, in comparison to the Upper Continental Crust (UCC), the sediments are significantly enriched in SiO_2, Fe_2O_3, Cr, and Ni and markedly depleted in Na_2O, MgO, CaO, MnO, and TiO_2. This is likely because feldspars were lost during chemical weathering. The sediments of the Atrai River are sub-arkosic in composition. The index of compositional variability (ICV) (0.95 to 1.35), and SiO_2/Al_2O_3 ratio (6.15 to 6.81) in the Atrai River sediments suggest poorly sorted grains, and low compositional and mineralogical maturity. The geochemical and petrographic discriminate diagrams and high Al_2O_3/TiO_2 values (20.57 to 32.55) indicate a felsic igneous provenance for the Atrai River sediments. They are mainly derived from granitic sources, with subordinate metamorphic and pre-existing sedimentary sources. The Higher Himalayas and the Lesser Himalayas are considered the possible source areas of the Atrai River sediments. Weathering indices (CIA, CIW, and PIA), as well as major and trace element discriminating diagrams, point to a weak-to-moderate degree of chemical weathering that may be prevalent in the source area under semi-arid climatic conditions. Petrographic and geochemical discriminating diagrams reveal an active margin tectonic setting for the Atrai River sediments.

Keywords Atrai River · Bengal Basin · Chemical weathering · Provenance · Southeastern Himalaya · Tectonic setting

Introduction

Provenance studies of clastic rocks and sediments are important to reveal the composition and chemical weathering of the source area complexes. The chemical composition of terrigenous sediments is frequently used to constrain insight into the transportation, degree of weathering, and tectonic setting of sedimentary basins (Al-Dousari et al. 2017; Al-Hemoud et al. 2022; Armstrong-Altrin et al. 2021; Armstrong-Altrin and Verma 2005; Bayon et al. 2015; Bhatia 1983; Condie 1967; Doronzo 2012; Hayashi et al. 1997; He et al. 2019; Herron 1988; Li et al. 2020; Noa Tang et al. 2020; Nesbitt and Young 1982, 1984; Rahman et al. 2020; Roser and Korsch 1986; Sayem et al. 2018; Suttner and Dutta 1986; Taylor and McLennan 1985; Viers et al. 2009; Wronkiewicz and Condie 1990). Chemical weathering, however, plays a significant role in the concentration of atmospheric CO_2, which ultimately affects the global climate (Ruddiman 2008). It also affects the nature of weathering products, and the solute chemistry of river and ocean water (Galy and France-Lenord 2001). Sediment is produced from parent rocks mainly through physical and

Responsible Editor: Domenico M. Doronzo

✉ Abu Sadat Md. Sayem
sayem8282@juniv.edu

[1] Department of Geological Sciences, Jahangirnagar University, Dhaka 1342, Bangladesh

[2] Institute of Mining, Mineralogy and Metallurgy (IMMM), Bangladesh Council of Scientific and Industrial Research (BCSIR), Joypurhat 5900, Bangladesh

chemical weathering, and certain elements remain immobile during several processes of sediment production, which is a good candid for source rock evaluation (Singh 2010). Thus, sediment geochemistry helps to infer the geological evolution of the source terrain. In addition, sediment geochemical analysis is also a useful indicator to decipher climate and tectonics in the catchment area.

Numerous studies have evaluated the provenance in the source area using the concentrations of mobile and immobile major elements and their ratios (Armstrong-Altrin et al. 2015, 2021; Hayashi et al. 1997; Hossain 2019; Long et al. 2012; Rahman et al. 2014a, 2014b; Roser and Korsch 1988; Taylor and McLennan 1985; Wronkiewicz and Condie 1990). The concentrations of certain trace elements are considered an excellent indicator of parent rock composition (Armstrong-Altrin et al. 2017; Armstrong-Altrin et al. 2021; Cullers 2000; Garver et al. 1996; Hossain 2019; Rosales-Lagarde et al. 2005; Torres-Sanchez et al. 2019). Various mobile and immobile major elemental ratios and diagrams demonstrate to infer the weathering intensity and climatic conditions in the sedimentary basin (Fedo et al. 1995; Harnois 1988; Kundu et al. 2016; McLennan 1989; Nesbitt and Young 1984; Parker 1970; Ranjan and Bannerjee 2009; Singh 2010; Suttner and Dutta 1986; Wronkiewicz and Condie 1990). Similarly, a number of geochemical discrimination diagrams have been employed to discriminate the tectonic settings of sedimentary basins, as it warrants attention to their indiscriminate application (Armstrong-Altrin and Verma 2005; Bhatia 1983; Nesbitt and Young 1984; Roser and Korsch 1986, 1988).

River sediments are important to lucidly understand the provenance and chemical weathering in the source area because rivers receive the weathering products through sedimentary processes. The Atrai River drains through diverse rock complexes, topography, and climate in the southeastern Himalaya. The intensity of chemical weathering in the Himalaya and its contribution to the solute load significantly influence global climate and ocean water chemistry. Thus, it offers a magnificent opportunity to understand the tectonics and climate of the derivative sediments. Numerous researchers investigated the provenance and tectonic setting of the Recent sediments based on petrography and geochemical concentrations in certain ways to understand mass balance by means of continental weathering (Armstrong-Altrin et al. 2021; Bayon et al. 2015; Hossain 2019; Li et al. 2020; Noa Tang et al. 2020; Viers et al. 2009). There are few provenance studies that use the mineralogy and geochemistry of river sediments from the southeastern Himalayan rivers. The Atrai River originates in the southeastern Himalaya and is considered one of the major tributaries of the mighty Brahmaputra River in the Bengal Basin (Fig. 1). Few studies have recently focused on the geochemical characterization of the recent river sediments in the

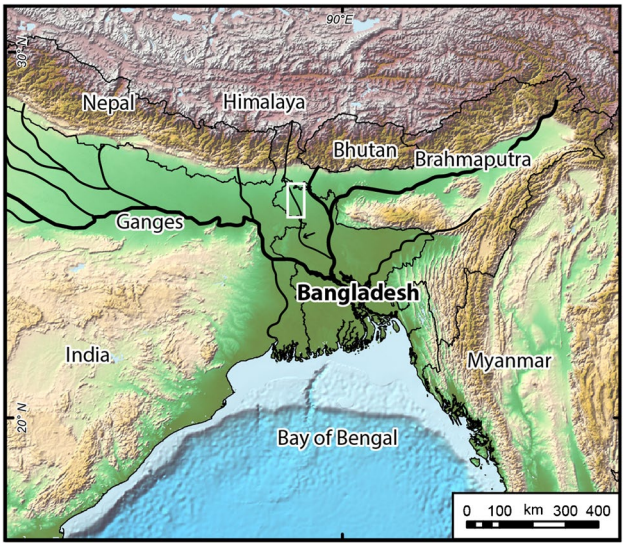

Fig. 1 Regional map showing the location of the Bengal Basin and surrounding regions. The black arrow indicates the location of the Atrai River and the white rectangle denotes the sampling sites in the study area

Bengal Basin (Bhuiyan et al. 2011; Abeden et al. 2017; Hossain 2019). Most of these studies were conducted in the middle or lower reaches of the Bengal Delta rivers, where sediment addition from the surrounding catchment as well as river bank erosion may affect the chemical composition of the investigated sediments. However, provenance studies based on geochemical and mineralogical composition from the upper reaches of the Bengal Basin rivers are poorly reported. In addition, the modal composition, besides the geochemistry, of river sediments is a reliable indicator for provenance analysis (Dickinson 1985). The main purpose of this study is to identify the geochemistry and modal composition of sediments from the upper reaches of the Atrai River in order to comprehend the provenance history and chemical weathering in the southeastern Himalaya.

Geological setting

The Bengal Basin has originated due to the collision between the Indian and Eurasian plates in the north and with the Burmese plate in the east (Abdullah et al. 2021, 2022; Najman et al. 2008; Yang et al. 2020) and has resulted in the extensive Himalayan and Indo-Burman Ranges, thereby loading the lithosphere to form flanking sedimentary basins (Uddin and Lundberg 1998). Due to the decreasing trend of elevation from north to south, nearly all of the rivers in the Bengal Basin flow due south. The Atrai River originates from the southeastern Himalaya, and flows through the northwest of the Bengal Basin (Fig. 1). It is one of the major feeder channels of the Teesta Megafan. The Atrai River flowing area

is divided into several distinct landforms: the Himalayan orogeny and the Teesta Alluvial Fan at the upper reaches, the Pleistocene Barind Tract in the middle and the floodplain deposit at the lower reaches of the river. The catchment area of the Atrai River comprises a diverse variety of rock compositions. Low to high grade metamorphic and granites are abundant in the Himalayan Orogeny (Critelli and Ingersoll 1994; Singh 2010; Uddin and Lundberg 1998). The Higher Himalaya Rocks consist of granites, medium- to coarse-grained banded gneiss, augen gneiss, magnetic gneiss, schists, and with leucogranites (Dasgupta et al. 2004; Singh 2010). Granites and low-grade metamorphic rocks such as gneiss, phyllites and schist dominate in the Lesser Himalayan Rocks (Dasgupta et al. 2004; Singh 2010). The Mio-Pliocene flysch sediments such as alteration of sandstone and shale, and mudstone (Siwalik) mark the southern margin of the Himalaya (Kundu et al. 2016). At its upper reaches, the Atrai River flows southward through the axial plain of the Teesta alluvial fan. The middle reaches of the river flow over the Pleistocene Barind Tract. The Barind Tract is entirely composed of clay and silty clay deposits. The lower reaches of the river pass through the unconsolidated Holocene Alluvium of the Ganges and Brahmaputra floodplains until its confluence with the Brahmaputra River (Fig. 1). At present, the total length of the Atrai River is approximately 390 km, and its depth ranges from 5 to 15 me. In the Atrai River catchment region, the mean annual precipitation is about 3000 mm/year, and the annual water discharge is close to 301 m^3/s (Rahman et al. 2011).

Materials and methods

For the purpose of this study, detailed field work was conducted in 2014 and 2019. Composite sediment samples (mixture of several subsamples from the same location) were collected from the channel bar deposits at intervals of about 3 km and at a depth of around 50 cm. A hand auger has been used to collect the samples. The raw and wet samples were preserved in the polyethylene bags before being brought to the laboratory for analytical investigation. For grain size analysis, prior to air drying, 100 g of each sample was sieved by a Row-Tap sieving machine for 20 min at the Department of Geological Sciences, Jahangirnagar University, Bangladesh. US Standard 18, 35, 60, 120, and 230 µm sieve meshes were used, and their size distributions were recorded based on Wentworth (1922). Textural parameters like mean, median, sorting, kurtosis and skewness were obtained by following Folk and Ward (1957).

Loose sediment samples were cooked with araldite to make them harden for petrographic analyses. The modal compositions of fifteen samples were determined by point counting of 500–600 grains per thin-section under a petrographic microscope fitted with a digital camera. For heavy mineral analysis (20 samples), sediment sizes of 1 to 0.063 mm were used for heavy separation. Ten grams of each sample were run for gravity separation by using Bromoform ($CHBr_3$) (density 2.89 g/cc at 20°C) following the procedure outlined by Mange and Maurer (1992). The heavy mineral separation and microscopic study of these minerals were carried out in the Department of Geological Sciences of Jahangirnagar University.

X-ray diffraction (XRD) of ten sediment samples was performed in order to identify clay minerals by VNR EXPLORER with CuKα radiation at 35 kV and 20 mA at the Wazed Miah Science Research Center, Jahangirnagar University, Bangladesh. Clay mineral fractions < 2 µm were obtained by the wet sieving of clay slurries and treated as air-dried, ethylene glycolated, and heated to 550 °C.

Nineteen sediment samples were analyzed for X-ray fluorescence (XRF) at the Institute of Mining, Minerals and Metallurgy (IMMM), BCSIR, Joypurhat, Bangladesh. At first, samples were treated with HCl to remove the organic particles, dried up in natural sunlight, and then crushed and powdered by using a planetary ball mill (PM-200, Retsch, Germany) for 20 min. Stearic acid was diluted with the powder samples at a ratio of 1:10 and pulverized for at least 2 min. The mixture was then ladled into an aluminum cap (30 mm) and compressed for 2 min using a manual hydraulic press at a pressure of 10 to 15 tons per square inch. The pellet was then prepared for X-ray analysis once pressure was steadily released. The major and trace element concentrations were obtained by X-ray fluorescence (XRF) spectrometry following the Goto and Tatsumi (1994, 1996) protocols that use the Rigaku ZSX Primus XRF machine equipped with an end window fitted with a 4 kW Rh-anode X-ray tube. A 40 kV voltage and a 60 mA current were applied to determine the heavy and light elements, respectively. USGS Rock Standards and Geological Survey of Japan (GSJ) Stream Sediment standards were used to obtain the results for this study. Analytical uncertainties for major and trace elements are about 2% and <10%, respectively. About 100 g of each sample was heated at 1000°C to obtain the loss of ignition (LOI) prior to the treatment.

Results

Petrography

The analyzed Atrai River sediments are dominantly medium-grained, angular to sub-angular, and moderately well sorted (Fig. 2). The framework grains are composed of monocrystalline quartz (Qm), polycrystalline quartz (Qp), K-feldspar, plagioclase, muscovite, biotite, and rock fragments (Fig. 2a–d, Table 1).

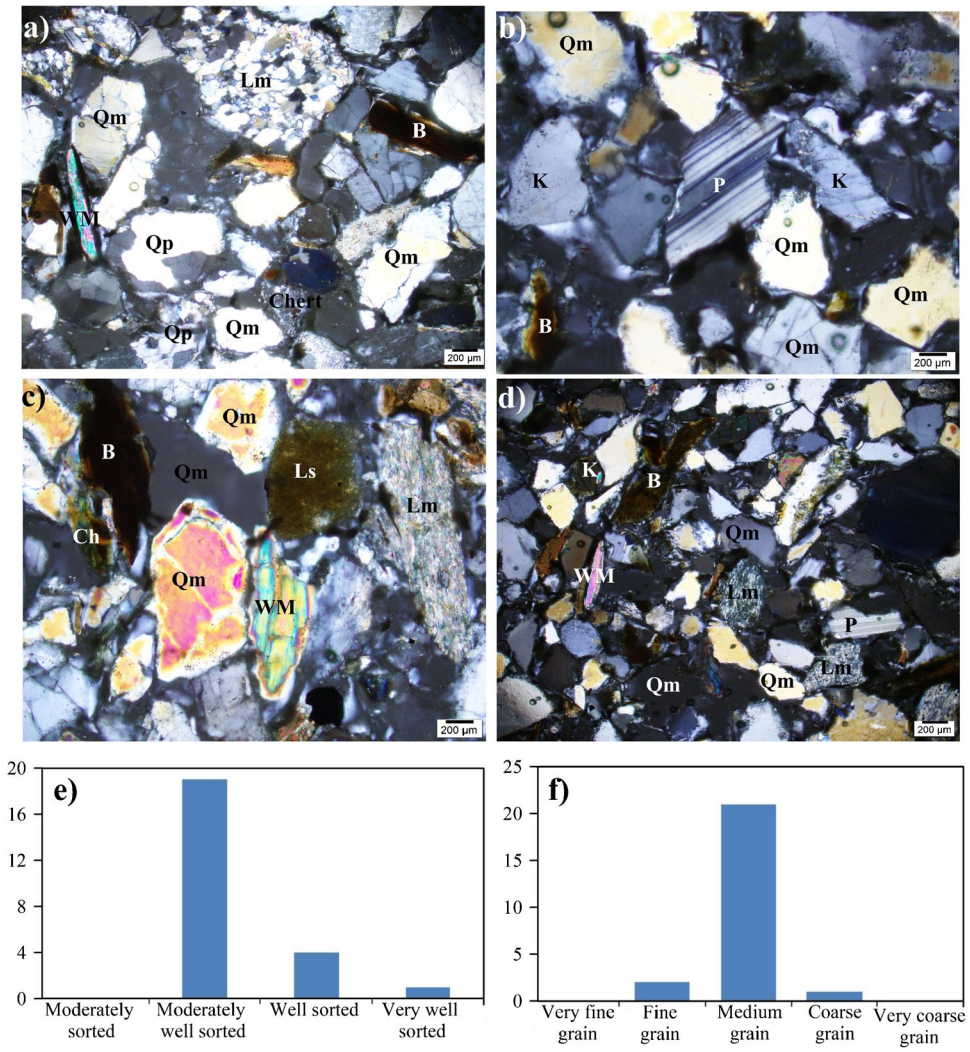

Fig. 2 Photomicrographs of the Atrai River sediments showing: **a–d** unstrained, angular to sub-angular monocrystalline quartz (Qm) and polycrystalline quartz (Qp), unaltered, angular to sub-angular K-feldspar (K) and plagioclase (P), white mica (WM), biotite (B), metamorphic lithic grain (Lm), sedimentary lithic grain (Ls), chlorite (Ch), and chert; **e** grain size distribution, and **f** sorting distribution of the Atrai River sediments

In the Atrai River sediments, quartz dominates all other framework minerals, making up an average of 65.5% of the total framework grains. The quartz grains are unstrained and angular to sub-angular in shape (Fig. 2a–d), and are dominated by Qm (56.4%) over Qp (9.1%). Feldspar grains are unaltered, angular to sub-angular (Fig. 2b, d) and account for an average of 13.9% of the total framework grains, where K-feldspar (8.5%) dominates over the plagioclase (5.4%). The two most prevalent types of K-feldspar are orthoclase and microcline, both present in the investigated sediments. Lithic fragments make up 5.96% of the total rock volume. Metamorphic lithic fragments (4.7%) dominate over sedimentary lithic grains (1.2%), and volcanic lithic grains are completely absent in the investigated sediments. Micas form a significant component in the analyzed sediments (Table 1). They are present as muscovite (white mica) and biotite (Fig. 2c, d), which comprise 4.87% and 3.91%, respectively.

The accessory heavy minerals occur in minor amounts (<1%) throughout the samples. It ranges from 0.3 to 0.8%. The heavy mineral grains are medium in size and show little abrasion. Both opaque and non-opaque heavy minerals are present in the Atrai River sediments. The non-opaque minerals include garnet, epidote, staurolite, sillimanite, kyanite, tourmaline, rutile, zircon, apatite, hornblende, etc. (Fig. 3a–k). The average concentration of the heavy minerals is shown in Fig. 3l. The accessory clay minerals are present in a very minor amount. Only illite, chlorite, and kaolinite are present as clay minerals in the studied sediments (Fig. 4).

Major element geochemistry

The major element concentrations of the Atrai River sediments are listed in Table 2. The results show a high concentration of SiO_2 in all the investigated samples, and it varies from 72.53 to 75.14%, with an average of 73.94%. Al_2O_3 ranges between 10.98 and 11.89%, with a mean value of 11.43%. The concentration of Fe_2O_3 is relatively high (average 6.23%) and attains a wide range from 3.30 to 7.44%. The average content of CaO, MgO, K_2O, and Na_2O is 1.44%, 0.81%, 3.66%, and 1.62%, respectively. $K_2O > Na_2O$ is

Table 1 Textural (Sayem et al. 2021) and framework mineralogical composition of the Atrai River sediments

Sample no	Mean	Sorting	Quartz		Chert	Feldspar		Mica		Ch	Lithic grains			Qt%	F%	L%
			Qm	Qp		K	P	WM	B		Ls	Lm	Lv			
ART1	1.51	0.67	59.52	10.37	1.07	8.58	7.43	3.00	3.00	1.07	1.07	3.72	0	77.33	17.45	5.22
ART2	1.30	0.47														
ART3	1.65	0.67	60.87	6.69	1.30	7.90	7.37	3.80	4.20	1.20	0.80	4.30	0.00	77.17	17.11	5.72
ART4	1.17	0.61														
ART5	1.24	0.76	59.50	6.54	1.81	6.90	3.62	6.70	3.96	1.35	0.40	5.43	0.00	72.40	18.09	9.51
ART6	1.61	0.53	54.32	8.86	1.35	10.06	6.06	4.64	3.48	1.74	1.16	7.32	0.00	77.35	15.80	6.85
ART7	1.16	0.63														
ART8	1.68	0.53	57.26	9.35	1.21	7.68	6.17	5.50	4.34	1.21	2.34	3.67	0.00	75.36	18.08	6.57
ART9	1.48	0.71	55.69	10.46	0.64	8.92	7.10	4.78	2.55	2.55	1.41	4.41	0.00	76.42	16.38	7.20
ART10	0.95	0.78	55.95	9.90	1.32	9.02	5.38	5.83	3.57	1.69	0.94	5.39	0.00	77.89	13.83	8.28
ART11	1.52	0.63	56.36	8.87	1.50	7.58	4.27	5.31	4.29	1.70	0.98	6.11	0.00	77.07	17.73	5.20
ART12	2.55	0.65														
ART13	1.83	0.53	53.09	9.61	2.60	10.32	4.70	5.55	4.20	1.32	1.20	3.21	0.00	77.87	16.51	5.62
ART14	2.17	0.66														
ART15	1.53	0.54	58.76	5.98	0.70	7.80	5.43	4.26	4.12	1.30	2.81	2.65	0.00	77.78	15.73	6.49
ART16	1.60	0.56														
ART17	1.35	0.58	56.41	7.21	1.23	7.44	6.31	4.98	6.20	0.85	0.91	3.77	0.00	79.76	15.53	4.71
ART18	1.33	0.54	53.87	13.76	2.33	9.52	4.10	5.57	2.91	0.78	1.03	3.10	0.00	78.73	13.48	7.79
ART19	1.40	0.40														
ART20	1.07	0.33	57.34	9.42	1.10	8.39	3.23	3.10	4.89	0.50	0.80	5.91	0.00	78.79	13.82	7.40
ART21	1.07	0.50														
ART22	1.30	0.48	54.78	11.43	0.90	7.45	4.32	4.50	4.89	1.00	1.40	4.90	0.00	80.58	12.49	6.92
ART23	1.57	0.60														
ART24	1.48	0.56	52.98	7.72	2.69	10.20	5.67	5.46	2.09	1.48	1.38	6.90	0.00	72.41	18.13	9.46
Average	**1.48**	**0.58**	**56.45**	**9.08**	**1.45**	**8.52**	**5.41**	**4.87**	**3.91**	**1.32**	**1.24**	**4.72**	**0.00**	**77.13**	**16.01**	**6.86**

Qm, monocrystalline quartz; *Qp*, Poly crystalline quartz; *K*, k-feldspar; *P*, plagioclase, *WM*, white mica; *B*, biotite; *Ls*, sedimentary lithic grains; *Lm*, metamorphic lithic grain; *Lv*, volcanic lithic grain; *Ch*, chlorite

consistent with the abundance of K-feldspar over plagioclase feldspar. TiO_2 is present in a minor amount, with an average value of 0.43%. The concentrations of MnO (avg. 0.10%) and P_2O_5 (avg. 0.09%) are very low in the Atrai River sediments.

In general, most of the major element concentrations in the Atrai River sediments are lower than the average values of the UCC (Fig. 5a), where the concentrations of SiO_2, Fe_2O_3, and K_2O are slightly enriched compared to the UCC values. The enrichment of SiO_2 relative to UCC indicates the abundance of quartz-rich sands. The depletion of Al_2O_3 suggests a low amount of clay components in the investigated sediments. Only illite, chlorite, and kaolinite clay minerals are evidenced by the bulk XRD analysis in the investigated sediments (Fig. 4). The enrichment of Fe_2O_3 relative to UCC in the analyzed samples is associated with the occurrence of heavy aluminosilicate minerals like garnet, epidote, amphibole, etc. (Fig. 3). The extreme depletion of Na_2O, MgO, and CaO compared to the average UCC is due to the continuous loss of plagioclase feldspar and calcite during the chemical weathering, whereas the slight enrichment of K_2O indicates the abundance of K-feldspar in the river sediments. MnO, TiO_2, and P_2O_5 show mostly stable chemical mobility in the source during chemical weathering.

The linear relationships of the major elements are calculated against Al_2O_3 and are shown in Table 3. The moderately negative correlation ($r = -0.442$) between SiO_2 and Al_2O_3 suggests that Si-rich materials are reduced gradually in the source rocks. The weak negative correlation between Al_2O_3 and Fe_2O_3 ($r = -0.185$) and Na_2O ($r = -0.117$) indicates a reduction of Fe in the clay fractions during chemical weathering, and the most leachable alkaline element (Na) reduces accordingly. The moderate positive correlations of CaO ($r = 0.443$), MgO ($r = 0.514$) and K_2O ($r = 0.428$) with Al_2O_3 suggest enrichment of mobile elements (Ca, Mg, and K) in the sediments. The moderately to strong positive correlations of Al_2O_3 with TiO_2 ($r = 0.531$) and P_2O_5 ($r = 0.792$) indicate the presence of heavy minerals, like apatite, garnet, amphibole (Fig. 3), and/or those associated with phyllosilicate (Fig. 4) in the investigated sediments. Very weak or no obvious correlation exists between MnO and Al_2O_3 in the Atrai River sediments.

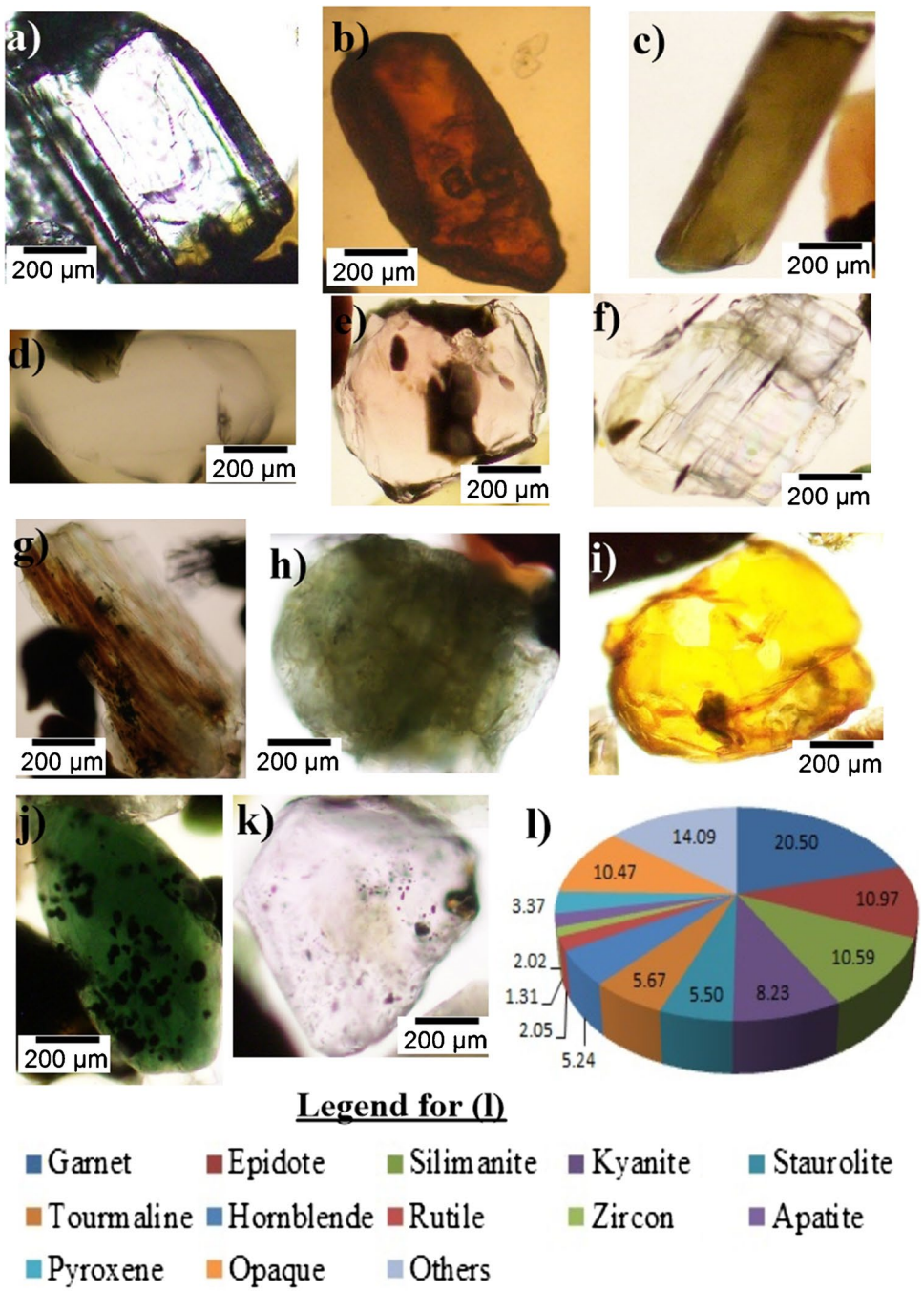

Fig. 3 Photomicrographs of heavy minerals of the Atrai River sediments showing: **a** zircon; **b** rutile; **c** tourmaline; **d** apatite; **e** garnet; **f** kyanite; **g** sillimanite; **h** epidote; **i** staurolite; **j** hornblende; **k** pyroxene; **l** pie chart of the average heavy mineral composition of the Atrai River sediments

Trace element geochemistry

The trace elements like Cr, Ni, Rb, Sr, Zr, Nb, Ba, and Zn are measured in the Atrai River sediments and reported in Table 2. Cr and Ni show extremely high concentrations (averages of 7465.3 ppm and 163.7 ppm, respectively) in the studied samples relative to the UCC. The Rb and Sr content ranges from 238 to 319 ppm (average 278.6 ppm) and 177 ppm to 232 ppm (average 196.7 ppm), respectively. The average concentrations of Zr and Zn are also much higher than the UCC value, and reported at 344.33 ppm and 169.7 ppm, respectively. The abundances of Nb and Ba are very negligible and are encountered only in a few sediment samples.

In general, almost all the trace element concentrations in the Atrai River sediments are enriched than the UCC, except for a slight depletion of Sr (Fig. 5b). This suggests that the trace elements are associated with accessory minerals. The enrichment of Cr, Ni, Rb, and Ba indicates that these elements are associated with feldspar and clay minerals. The

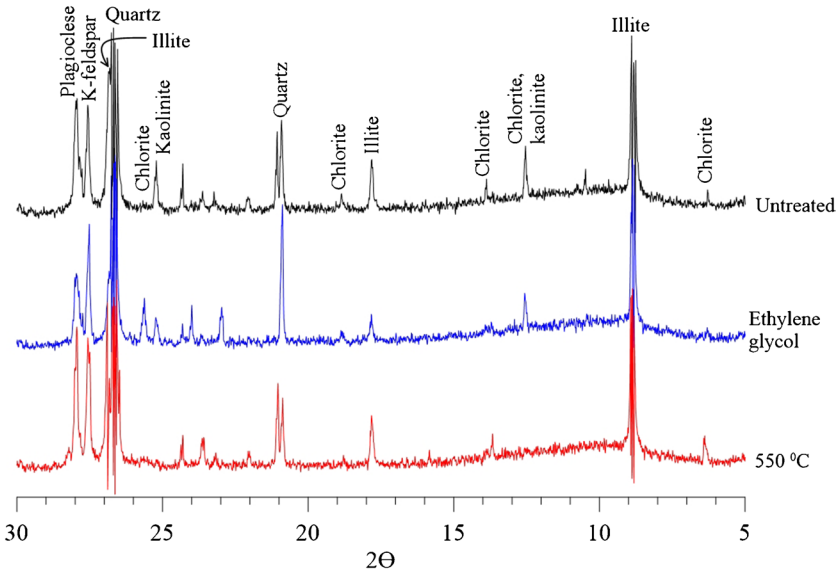

Fig. 4 Clay separate (<2 µm) XRD diffractogram (glycolated) of the Atrai River sediments (sample ART 7)

depletion of Sr reflects weathered feldspar in the source, while the enrichment of Zr suggests an abundance of zircon in the investigated sediments. The transitional metal Zn is slightly enriched in comparison to UCC. The trace element concentrations of the Atrai River sediments show a weak positive correlation with Al_2O_3, except for Cr and Zn (Table 3). The positive correlations of Al_2O_3 with Rb (r = 0.069) and Sr ($r = 0.448$) reflect the abundance of K-feldspar (Table 1) and the presence of clay minerals (Armstrong-Altrin et al. 2013) in the studied sediments. The weak positive correlation between Zr and Al_2O_3 ($r = 0.226$) indicates enrichment of Zr-rich accessory minerals like zircon in the Atrai River sediments. A very weak positive correlation of Ni with Al_2O_3 ($r = 0.068$) indicates an influx of Ni-rich silicate minerals. The significant negative correlation between Al_2O_3 and Cr ($r = 0.385$) reflects a lower abundance of clay minerals (Fig. 4) in the investigated samples.

Discussion

Sediment classification and maturity

The SiO_2, Al_2O_3, and their ratios are commonly used in sediment classification and maturity as their abundance directly reflects the quartz, feldspar and clay contents in the sediments. The alkali contents of Na_2O and K_2O are also applicable for sandstone classification and index of chemical maturity measure of the feldspar content. Pettijohn et al. (1972) proposed a classification scheme for clastic sedimentary rocks based on log (SiO_2/Al_2O_3) vs. log (Na_2O/K_2O) ratios. On this diagram, the Atrai River sediments are classified as sub-arkosic type (Fig. 6a). Similarly, based on the QFL ternary diagram (Potter 1978), the analyzed samples are also classified as sub-arkose in nature (Fig. 6b). However, arkose to sub-arkose composition indicates that the sediments are texturally and mineralogically immature (Zaid 2015). Potter (1978) introduced a chemical maturity index of $SiO_2/A1_2O_3$ to obtain sediment maturity. Generally, $SiO_2/A1_2O_3$ index of mature sands show moderately well positive correlation with total quartz content (Qt) and vice versa. The relationship between $SiO_2/A1_2O_3$ and Qt (Fig. 7a) shows a very weak negative correlation (−0.04), which indicates that Atrai River sediments are immature. On the other hand, the alkali content ($Na_2O + K_2O$) is very much applicable as an index of chemical maturity and also a measure of the feldspar content (Pettijohn et al. 1972). Mature and well-rounded sands ($Na_2O + K_2O$) is negatively correlated with (F+Lt). The Atrai River sediments show (Fig. 7b) a weak positive (0.11) correlation between ($Na_2O + K_2O$) and (F+Lt). Thus, this result also suggests immature sediments for the studied samples. In addition, the low concentration of ultra-stable minerals like zircon, tourmaline, and rutile (Fig. 3I) and the low ZTR index (Sayem et al. 2021) of the Atrai River detritus indicate that the sediments are mineralogically immature.

The sediments maturity can be well explained by using index of compositional variability (ICV = (Fe_2O_3+K_2O+Na_2O+ CaO + MgO + TiO_2)/Al_2O_3) (Cox et al. 1995). The higher ICV values (>0.84) reflect enrichment of major rock-forming minerals like feldspars, amphiboles, and pyroxenes as well as the textural immaturity of sediments. On the other hand, the lower ICV values (<0.84) reflect clay minerals like kaolinite, illite, and muscovite and imply recycling and/or intense weathering in the source area. The ICV values of the investigated sediments range from 0.95 to 1.35 (Table 2), indicating that the sediments are geochemically immature and associated with major rock-forming minerals. In addition, the ratio of SiO_2/

Table 2 Major and trace element concentrations of the Atrai River sediments

Sample no	ATR1	ATR2	ATR3	ATR4	ATR5	ATR6	ATR7	ATR8	ATR9	ATR10	ATR11	ATR 12	ATR 13	ATR 15	ATR 17	ATR 18	ATR 20	ATR 22	ATR 24	Average
Major elements (%)																				
SiO_2	73.81	75.14	73.29	74.73	74.40	72.53	73.24	73.43	74.25	74.92	73.17	74.47	74.01	73.47	73.33	74.58	73.82	74.22	74.04	73.94
Al_2O_3	11.43	11.54	11.39	10.98	11.34	11.80	11.34	11.89	11.75	11.09	11.33	11.48	11.18	11.57	11.61	11.42	11.41	11.46	11.21	11.43
Fe_2O_3	6.44	3.30	6.74	6.43	6.27	6.67	7.11	6.30	6.20	6.39	7.44	4.87	6.58	6.47	6.70	6.30	6.15	5.02	6.92	6.23
CaO	1.49	1.36	1.51	1.30	1.31	1.65	1.59	1.57	1.44	1.18	1.50	1.42	1.40	1.48	1.58	1.31	1.46	1.43	1.34	1.44
MgO	0.82	0.68	0.83	0.74	0.80	0.95	0.79	0.95	0.76	0.79	0.83	0.75	0.79	0.87	0.87	0.77	0.79	0.76	0.81	0.81
Na_2O	1.65	1.49	1.95	1.60	1.65	1.82	1.69	1.53	1.27	1.50	1.63	1.57	1.78	1.73	1.61	1.38	1.60	1.72	1.56	1.62
K_2O	3.61	3.74	3.64	3.70	3.69	3.89	3.57	3.67	3.70	3.62	3.42	3.68	3.67	3.79	3.62	3.66	3.55	3.69	3.52	3.66
MnO	0.11	0.08	0.11	0.09	0.08	0.11	0.12	0.10	0.09	0.09	0.13	0.09	0.10	0.09	0.11	0.09	0.11	0.10	0.11	0.10
TiO_2	0.56	0.38	0.44	0.36	0.38	0.48	0.46	0.47	0.44	0.34	0.46	0.47	0.40	0.43	0.46	0.39	0.46	0.41	0.40	0.43
P_2O_5	0.09	0.08	0.10	0.07	0.08	0.10	0.09	0.09	0.09	0.07	0.08	0.08	0.08	0.09	0.09	0.08	0.08	0.09	0.08	0.09
LOI	0.89	0.96	1.24	0.97	1.17	1.08	1.19	0.90	0.77	1.07	1.09	1.11	0.00	0.00	0.00	0.00	0.55	1.11	0.00	0.74
Na_2O/ K_2O	0.46	0.40	0.54	0.43	0.45	0.47	0.47	0.42	0.34	0.41	0.48	0.43	0.48	0.46	0.44	0.38	0.44	0.47	0.38	0.44
Al_2O_3/ TiO_2	20.57	30.22	26.04	30.28	30.22	24.67	24.52	25.44	26.69	32.55	24.68	24.50	27.96	27.11	24.99	29.24	28.03	27.99	26.05	26.93
K_2O/ Na_2O	2.19	2.52	1.87	2.31	2.24	2.14	2.11	2.40	2.91	2.42	2.10	2.35	2.07	2.18	2.25	2.65	2.25	2.15	2.63	2.30
Al_2O_3/ SiO_2	0.15	0.15	0.16	0.15	0.15	0.16	0.15	0.16	0.16	0.15	0.15	0.15	0.15	0.16	0.16	0.15	0.15	0.15	0.16	0.15
SiO_2/ Al_2O_3	6.46	6.51	6.44	6.81	6.56	6.15	6.46	6.18	6.32	6.76	6.46	6.48	6.62	6.35	6.31	6.53	6.61	6.47	6.25	6.46
F1	−2.15	−4.27	−1.61	−.21	−2.18	−1.94	−1.35	−2.09	−2.16	−2.23	−1.06	−2.37	−1.91	−2.06	−1.72	−2.19	−1.64	−2.10	−2.12	−2.07
F2	−0.13	0.63	0.22	−0.17	−0.10	0.37	−0.26	−0.30	−0.47	−0.55	−0.72	−0.03	0.02	0.14	−0.28	−0.51	−0.64	0.15	−0.38	−0.16
CIA	55.62	56.82	54.11	55.41	56.01	54.24	54.59	56.59	58.91	57.02	55.95	56.22	54.74	55.09	55.74	57.54	56.52	55.44	57.29	55.99
PIA	59.08	61.35	56.57	59.08	59.94	56.92	57.80	60.60	63.28	61.75	59.38	60.19	57.76	58.36	59.21	62.55	60.59	58.87	61.90	59.75
CIW	68.70	70.97	66.56	69.46	69.79	67.25	67.52	69.80	72.35	71.40	68.48	69.82	67.95	68.47	68.67	71.89	69.96	68.71	71.04	69.41
ICV	1.274	0.949	1.326	1.288	1.243	1.31	1.342	1.219	1.176	1.247	1.349	1.111	1.307	1.277	1.279	1.21	1.229	1.136	1.299	1.24
Trace elements (ppm)																				
Ni	0.0	134.0	184.0	153.0	230.0	243.0	146.0	133.0	139.0	173.0	167.0	167.0	67.0	168.5	170.0	194.5	191.5	236.5	212.8	163.7
Zn	144.0	138.0	215.0	246.0	149.0	134.0	185.0	148.0	139.0	142.0	190.0	190.0	141.0	230.5	166.0	159.5	197.5	141.5	169.0	169.7
Rb	258.0	264.0	294.0	316.0	259.0	319.0	238.0	273.0	274.0	274.0	274.0	274.0	261.0	305.0	274.0	278.5	287.5	289.0	280.9	278.6
Sr	203.0	187.0	214.0	185.0	190.0	232.0	177.0	201.0	192.0	187.0	191.0	191.0	195.0	199.5	189.0	204.5	187.5	211.0	200.9	196.7
Zr	319.0	364.0	365.0	293.0	338.0	425.0	384.0	364.0	292.0	319.0	303.0	303.0	341.5	329.0	311.0	404.5	315.5	381.5	389.2	344.3
Nb	0.0	0.0	0.0	0.0	0.0	0.0	0.0	45.0	42.0	0.0	0.0	0.0	0.0	0.0	0.0	0.0	0.0	0.0	65.0	8.0
Ba	1065.0	1177.0	0.0	0.0	0.0	0.0	0.0	1226.0	0.0	807.0	0.0	0.0	1121.0	0.0	403.5	0.0	0.0	0.0	121.2	311.6
Cr	6848.0	6068.0	7768.0	7692.0	8729.0	6775.0	7779.0	6200.0	6050.0	8339.0	8485.0	8485.0	6458.0	7730.0	8412.0	7277.0	8210.5	7752.0	6784.0	7465.3

NB: *F1*, Discriminant function 1; *F2*, Discriminant function 2; *CIA*, Chemical Index of Alteration; *PIA*, Plagioclase Index of Alteration; *CIW*, Chemical Index of Weathering; *ICV*, Index of compositional variability

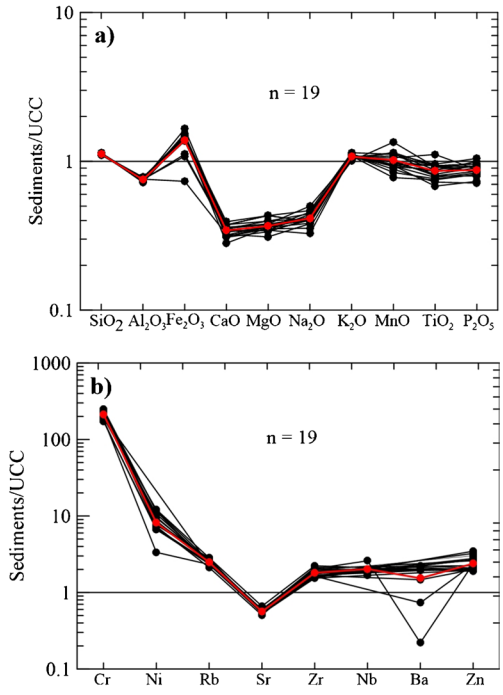

Fig. 5 **a** Normalized major element concentrations of the Atrai River sediments plotted against UCC; **b** normalized trace element concentrations of the Atrai River sediments plotted against UCC. Reference values for UCC are taken from Taylor and McLennan (1985). The solid red line represents the average concentrations of the element in the investigated samples

Al_2O_3 is also used to understand the compositional maturity of clastic sediments (Potter 1978; Roser et al. 1996). The SiO_2/Al_2O_3 ratio of the Atrai River sediments ranges from 6.15 to 6.81 with an average value of 6.61, which suggests that the sediments are moderately mature. Moreover, the bivariate plot of ICV vs. CIA (chemical index of alteration; Long et al. 2012) (Fig. 8) indicates that the studied sediments are compositionally immature. The angular to sub-angular framework grains (Fig. 2a–d) and fresh feldspars (Fig. 2b, d) are also supportive of immature sediments. The immature to moderately mature nature of recent river sediments is also reported in previous studies from the Ganges, Yarlung Zangbo (upper Brahmaputra), and Meghna River sediments (Hossain 2019; Huyan et al. 2021; Singh 2010).

Provenance

The quantitative petrography offers crucial information about the nature of the source area lithology. The textural and mineralogical characteristics of the Atrai River sediments (such as medium grained, moderately sorted, high proportion of quartz, dominance of K-feldspar over plagioclase, and unstrained monocrystalline quartz) suggest a weathered crystalline granitic/plutonic source terrain (Roser et al. 1996; Zaid 2015). However, the angular to sub-angular quartz and feldspar grains (Fig. 2a–d) and rarely rounded

Table 3 Correlation matrixes of the major oxides and selected trace elements of the Atrai River sediments (the negative correlations are shaded to gray)

	SiO_2	Al_2O_3	Fe_2O_3	CaO	MgO	Na_2O	K_2O	MnO	TiO_2	P_2O_5	Rb	Sr	Zr	Zn	Ni	Cr
SiO_2	1.000															
Al_2O_3	-0.442	1.000														
Fe_2O_3	-0.614	-0.185	1.000													
CaO	-0.889	0.666	0.271	1.000												
MgO	-0.811	0.514	0.558	0.654	1.000											
Na_2O	-0.576	-0.117	0.269	0.432	0.384	1.000										
K_2O	0.029	0.428	-0.381	0.102	0.152	0.120	1.000									
MnO	-0.720	-0.003	0.582	0.570	0.392	0.367	-0.604	1.000								
TiO_2	-0.653	0.531	0.210	0.785	0.469	0.207	-0.111	0.524	1.000							
P_2O_5	-0.780	0.792	0.165	0.853	0.658	0.415	0.352	0.606	0.606	1.000						
Rb	-0.194	0.069	0.079	0.082	0.301	0.278	0.443	-0.001	0.019	0.201	1.000					
Sr	-0.413	0.448	-0.098	0.330	0.505	0.408	0.531	0.076	0.189	0.638	0.585	1.000				
Zr	-0.336	0.226	0.093	0.249	0.368	0.294	0.258	0.144	0.074	0.376	0.040	0.665	1.000			
Zn	-0.205	-0.095	0.115	0.165	-0.015	0.162	-0.273	0.312	0.314	-0.078	0.075	-0.366	-0.307	1.000		
Ni	-0.083	0.068	0.260	0.021	0.109	0.094	0.144	0.003	-0.393	0.098	0.454	0.278	0.386	0.099	1.000	
Cr	-0.039	-0.385	0.228	-0.130	-0.035	0.246	-0.342	0.161	-0.093	-0.247	0.030	-0.284	-0.331	0.441	0.397	1.000

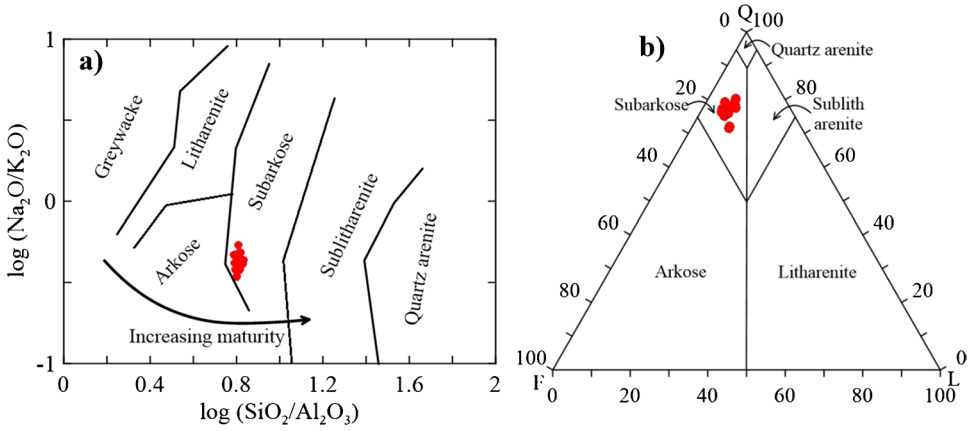

Fig. 6 Classification of the Atrai River sediments: **a** geochemical classification of log (SiO_2/Al_2O_3) vs. (Na_2O/K_2O) after Pettijohn et al. 1972; **b** QFL ternary diagram after Potter (1978)

to sub-rounded zircon and tourmaline grains imply granitic sources with sub-ordinate pre-existing sedimentary and meta-sedimentary rocks. The modal compositions of the investigated sediments are plotted in the QtFL and QmFLt diagrams (Dickinson et al. 1983). On these diagrams (Fig. 9), the samples fall along the boundary between craton interior, transitional continental and recycled orogen provenances.

The chemical composition of clastic sediments is a useful tool to discriminate their provenance (Condie et al. 1992; Cullers 1995; Roser and Korsch 1986, 1988; Taylor and McLennan 1985). The major elements-based discrimination function diagram proposed by Roser and Korsch (1988) is widely used to infer provenance, where the river-derived sediments are discriminated into felsic, intermediate, mafic, and quartzose sedimentary sources. On this diagram (Roser and Korsch 1988), the Atrai River sediments indicate dominantly felsic igneous sources (Fig. 10a), which is consistent with the bivariate plot of TiO_2 vs. Zr (Fig. 10b). However, the ICV values (> 0.84) for the investigated sediments demonstrate first-cycle deposition (Cox et al. 1995). In addition, the abundance of unaltered feldspar and angular to sub-angular grains (Fig. 2a–d) suggests quick deposition of sediments near the sources.

Based on the Al_2O_3/TiO_2 ratio, Hayashi et al. (1997) differentiated the igneous rocks into mafic, intermediate, and felsic, with the values ranging from ~3 to 8, ~8 to 21 and ~21 to 70, respectively. The higher Al_2O_3/TiO_2 values (ranges from 20.57 to 32.55) indicate that the studied sediments originated primarily from felsic igneous provenance. In addition, the river sediments are discriminated as felsic, intermediate, and mafic sources based on SiO_2 content (Le Bas et al. 1986). According to this diagram, the Atrai River sediments are classified as felsic sources (Fig. 10c). The ternary plot of CaO-Na_2O-K_2O (Condie 1967) for the Atrai River sediments reflects granitic and quartz monzonitic composition (Fig. 10d). In this study, the average values of SiO_2/Al_2O_3 and K_2O/Na_2O ratios are 6.47 and 2.29, respectively (Table 2). These values are relatively higher than those of the UCC (4.34 and 0.87), which indicate that the investigated sediments were derived from crustal granitic sources of the Higher Himalaya (Taylor and McLennan

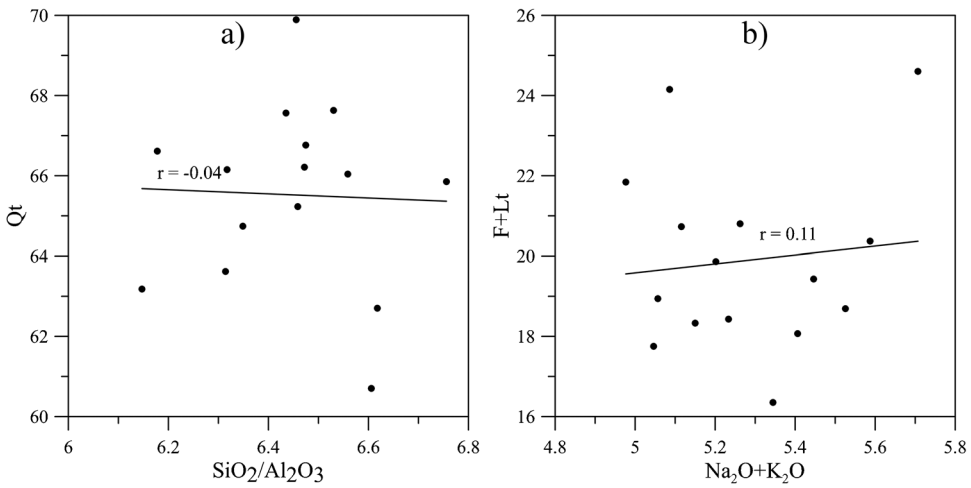

Fig. 7 Bivariate plots showing the relationships between **a** SiO_2/Al_2O_3 vs. total quartz (Qt); and **b** (Na_2O_3+K_2O) vs. feldspar plus total lithic grains (F+Lt)

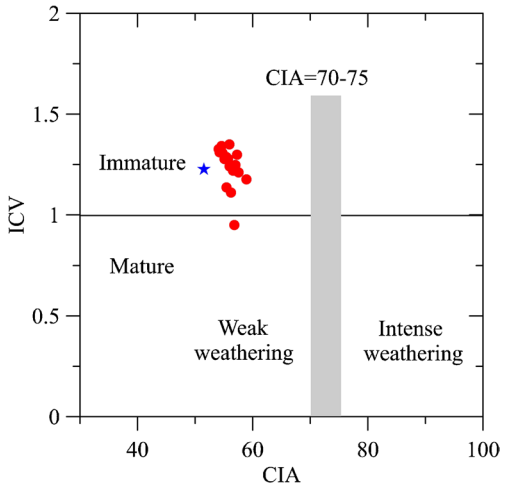

Fig. 8 Compositional maturity diagram of ICV vs. CIA (Long et al. 2012) reflects the sediments are compositionally immature and weak chemical weathering in the source area. (Blue color star symbol indicates UCC value as a reference point)

1985). Furthermore, the occurrence of more than 73% SiO_2 indicates that the Atrai River sediments are quartz-rich and derived from quartz-rich crystalline provenance. In addition, Zaid (2015) postulated that higher K_2O/Na_2O values reflected granitic source rock. This result is also confirmed by the occurrences of illite and kaolinite and the absence of smectite clay minerals (Fig. 4), which were derived from the weathered granitic rocks. The concentrations of Cr and Ni are widely used to discriminate mafic over felsic sources (McLennan et al. 1993; Wronkiewicz and Condie 1987). Higher contents of Cr (>150 ppm) and Ni (>100 ppm) (Table 2) are indicative of ultramafic sources (Garver et al. 1996). In this study, the higher concentrations of (average 7465 ppm) and Ni (average 163 ppm) (Table 2) indicate denudation of ultramafic rocks in the southeastern Himalaya. The presence of pyroxene (3.37%) and opaque minerals (10.47%) (Fig. 3I) also indicate a mafic source. Thus, the petrographic and geochemical characteristics suggest a dominant felsic igneous with sub-ordinate mafic, and sedimentary and meta-sedimentary sources for the Atrai River sediments. A recent heavy mineral study (Sayem et al. 2021) also suggests acid igneous, metamorphic, and basic igneous provenances for the Atrai River sediments.

To reveal the possible source area and source lithology, the major elements (K_2O, Na_2O, CaO, TiO_2, Fe_2O_3, Al_2O_3, and SiO_2) of the Atrai River sediments are plotted on different binary diagrams (Singh 2010). These diagrams (Fig. 11a–c) clearly suggest that the investigated sediments were derived from the Higher Himalayan Crystalline Series (granites/gneiss/schist) as well as the Lesser Himalayan Series (granite/gneiss/phyllite/schist).

Source area weathering

The geochemical composition of sediments is an excellent indicator of the weathering states in the source area. Several indices have been used to measure the chemical weathering intensity of sediments (Cullers 2000; Fedo et al. 1995; Harnois 1988; Nesbitt and Young 1982; Parker 1970). Generally, weathering indices make a comparison between a relatively stable mineral or chemical compound and one that is readily removed by weathering. In this study, a number of weathering indices (CIA, PIA, and CIW) were applied to assess the weathering condition in the source area, and their corresponding values are listed in Table 2.

The Chemical Index of Alteration (CIA) is a widely accepted weathering index and gives an indication of the degree of weathering in the source region (Nesbitt and Young

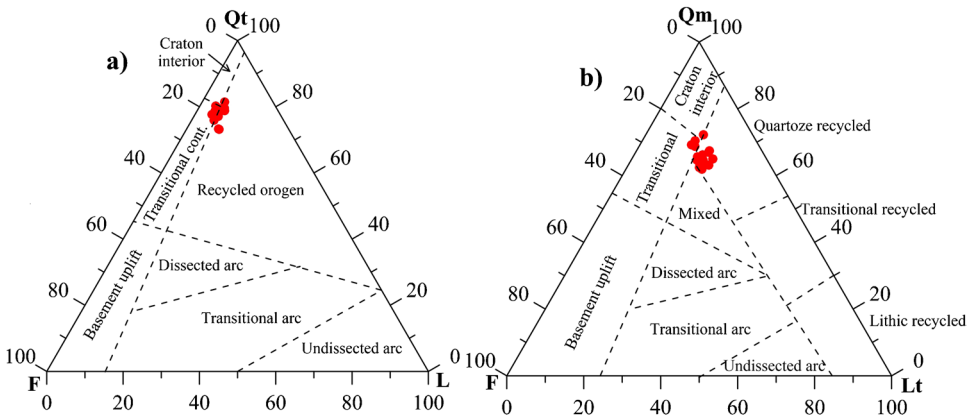

Fig. 9 QtFL **a** and QmFLt **b** ternary diagrams for the Atrai River sediments, after Dickinson et al. (1983)

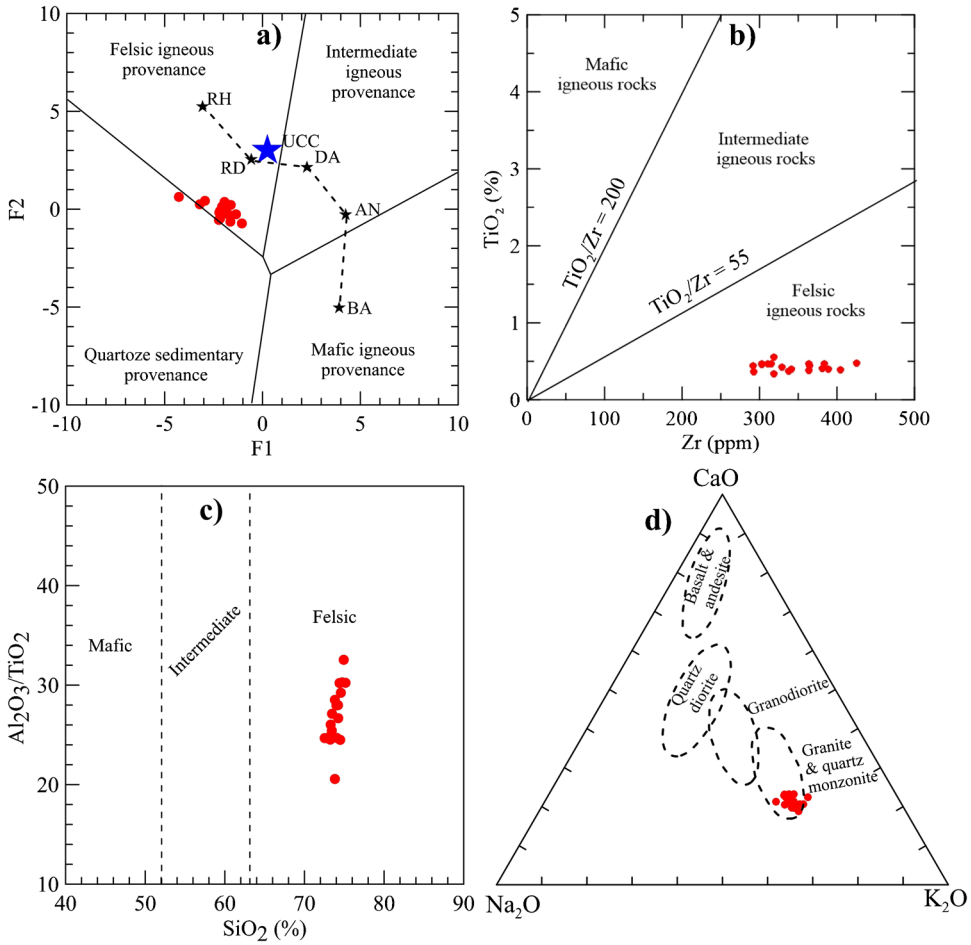

Fig. 10 Provenance discriminant diagrams: **a** discriminant factor F1 vs F2 (Roser and Korsch 1988) for the Atrai River sediments in the northwest Bengal Basin (BA — Basalt, AN — Andesite, DA — Dacitee, RD — rhyodacite, R-rhyolite), UCC — upper continental crust); **b** TiO_2 vs. Zr for the Atrai River sediments (Hayashi et al. 1997); **c** Al_2O_3/TiO_2 vs. SiO_2 bivariate plot for the Atrai River sediments (Le Bas et al. 1986); **d** ternary diagram of CaO–Na_2O–K_2O for the Atrai River sediments (Condie 1967)

1982). It indicates the progressive alteration of plagioclase and potassium feldspar to clay minerals, with a CIA value of nearly 100 for kaolinite and chlorite and 70–75 for average shale. High CIA values (76–100) indicate the removal of labile elements (Na, K, and Ca) in comparison to the more stable elements (Al and Ti) in the weathering profile (Nesbitt and Young 1982). Such high CIA values infer intensive chemical weathering as well as a hot and humid climate. On the contrary, low values (50 or less) indicate an unweathered source area under cold and arid climatic conditions. The CIA values for the Atrai River sediments range from 54.11 to 58.91, with an average value of 55.99. This result implies that the sediments were likely derived from weak to moderate weathering profiles under semi-arid and/or sub-humid

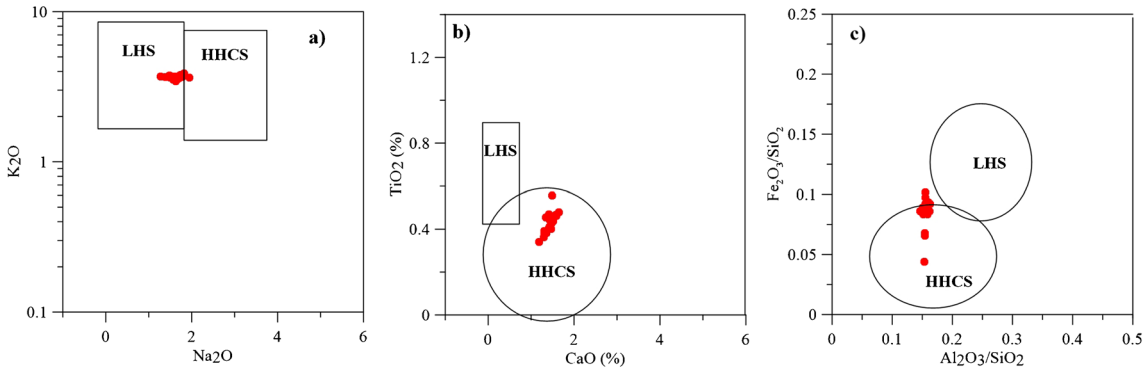

Fig. 11 Binary plots **a–c** of the major elements clearly show that the Higher Himalaya Crystalline Series (HHCS) and the Lesser Himalaya Series (LHS) acted as the dominant source for the Atrai River sediments (The HHCS and LHS fields are adopted after Singh 2010.).

climatic conditions. Similarly, the Chemical Index of Weathering (CIW) measures the extent of conversion of feldspar to clay in the weathering profile (Fedo et al. 1995; Nesbitt and Young 1984). CIW values up to 50 indicate unweathered rocks, and higher values reflect strong chemical weathering (Harnois 1988). The river sediments in this study reflect a narrow range from 65.56 to 72.35, with an average value of 69.41, indicating moderate chemical weathering in the source area. Plagioclase Index of Alteration (PIA) is proposed by Fedo et al. (1995) as an alternative to CIW and is applied to understand the plagioclase weathering in the source region. PIA values range from ≤ 50 for the fresh, unweathered rocks to 100 for the optimum weathered rocks. The PIA values of the Atrai River sediments range between 56.57 and 63.28 with a mean value of 59.75, which implies weak-to-moderate chemical weathering of the source area.

The bivariate plot of K_2O vs. Rb (Wronkiewicz and Condie 1990) for the Atrai River sediments is clustered a bit away from the average crustal line (K/Rb = 230) and close to the late-stage granite, which indicates moderate chemical weathering in the source area (Fig. 12a). However, the ICV vs. CIA plot reflects weak chemical weathering for the Atrai River sediments (Fig. 8). The results of this relatively weak-to-moderate weathering intensity for the investigated sediments are identical for the Himalayan River sediments as well as the Himalayan rock complexes (Bhuiyan et al. 2011; Hossain 2019; Huyan et al. 2021; Singh 2010). The rate of tectonic uplift controls the chemical weathering in the source area (Wronkiewicz and Condie 1987). In addition, hot and humid climates intensify chemical weathering (Jacobson et al. 2003; Sayem et al. 2018) and vice versa. The weak-to-moderate chemical denudation reflected by the above weathering indices suggests a relatively cold and semi-arid climatic condition in the source area. Moreover, the elemental ratios of SiO_2 vs. (Al_2O_3+Na_2O+K_2O) reflect semi-arid climatic condition (Fig. 12b) in the southeastern Himalaya.

Tectonic setting

Detrital sandstone compositions have been linked to significant provenance types and tectonic settings like stable cratons, basement uplifts, magmatic arcs, and recycled orogens (Dickinson and Suczek 1979; Dickinson et al. 1983). On QtFL and QmFLt ternary diagrams, the investigated samples fall at the boundary between craton interior, transitional continental, and recycled orogen (Fig. 9a, b). This result implies that the sediments were derived from continental margin prior to collision and deposited in the foreland basin. However, the unaltered and angular to sub-angular feldspar grains (Fig. 2b, d), and sub-arkosic composition (Fig. 6a, b) indicate quick deposition of sediments due to rapid uplift of the source area in a collisional regime.

The geochemical composition of terrigenous sediments reflects different tectonic settings of provenance terrains (Armstrong-Altrin et al. 2021; Bhatia 1983; Roser and Korsch 1986; Verma 2015; Verma and Armstrong-Altrin 2013). Several discriminate function diagrams were used to understand the tectonic setting for the Atrai river sediments. The discriminate function diagram of SiO_2 vs. log (K_2O/Na_2O) (Roser and Korsch 1986) suggests an active margin tectonic setting (Fig. 13a) for the Atrai River sediments. A similar result is obtained from the SiO_2/Al_2O_3 vs. log (K_2O/Na_2O) diagram (Roser and Korsch 1986) (Fig. 13b). Verma and Armstrong-Altrin (2013) proposed new tectonic discriminate function diagrams DF1 $(Arc\text{-}Rift\text{-}Col)_{m1}$ vs. DF2 $(Arc\text{-}Rift\text{-}Col)_{m1}$ and DF1 $(Arc\text{-}Rift\text{-}Col)_{m2}$ vs. DF2 $(Arc\text{-}Rift\text{-}Col)_{m2}$ for clastic sediments, where the sediments on the active margin represent the arc and collision settings, while the sediments in the passive margin indicate the rift setting (Verma and Armstrong-Altrin 2013). On these diagrams (Fig. 13c, d), the investigated sediments are scattered in the collision field and continental arc field, respectively, which implies an active margin tectonic setting for the Atrai River sediments.

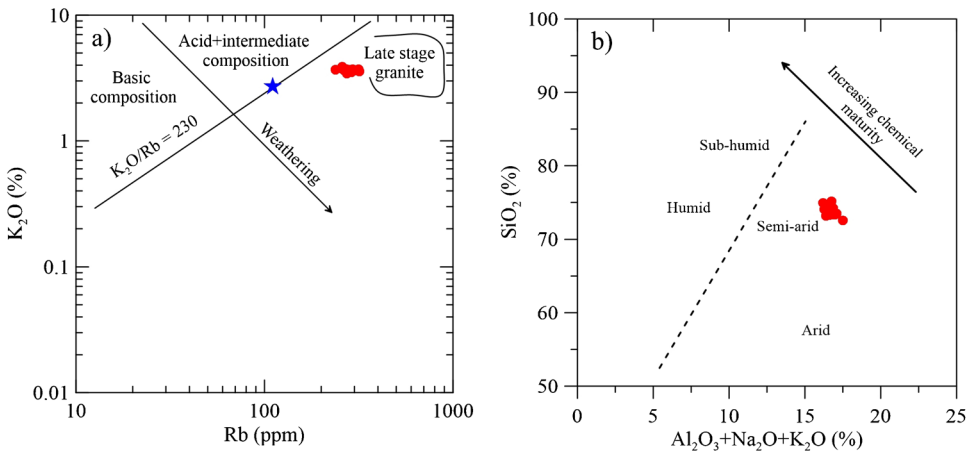

Fig. 12 **a** The bivariate plot of K_2O vs. Rb after Wronkiewicz and Condie 1990, where, the K/Rb=230 line indicates the average crustal ratio. Star symbol indicates the value of UCC (Taylor and McLennan 1985); **b** SiO2 vs. (Al_2O_3+Na_2O+K_2O) plot for the Atrai River sediments (after Suttner and Dutta 1986)

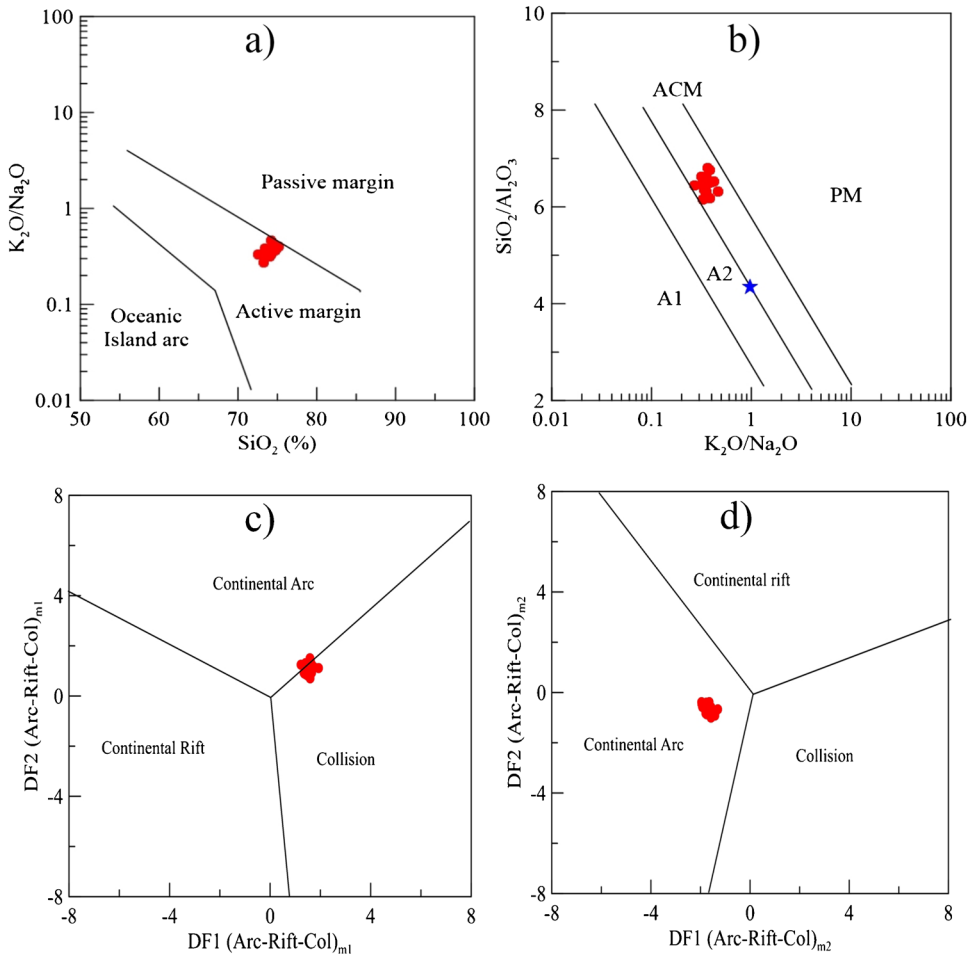

Fig. 13 Tectonic discrimination diagrams for the Atrai River sediments: **a** SiO_2 vs. log (K_2O/Na_2O) (after Roser and Korsch 1986); **b** SiO_2/Al_2O_3 vs. log (K_2O/Na_2O) (after Roser and Korsch 1986) [ACM — active continental margin; PM — passive margin; CIA — continental island arc; OIA — oceanic island arc; A1 — evolved arc setting, basaltic and andesitic detritus; A2 — evolved arc setting, felsic-plutonic detritus]; **c–d** new tectonic discriminate function diagrams DF1 (Arc-Rift-Col)$_{m1}$ vs. DF2 (Arc-Rift-Col)$_{m1}$ and DF1 (Arc-Rift-Col)$_{m2}$ vs. DF2 (Arc-Rift-Col)$_{m2}$ (after Verma and Armstrong-Altrin 2013)

Comparison of the Atrai River sediments with the other major rivers in the southern Himalaya

A number of large rivers originate from the southern Himalaya, namely the Ganga River, the Brahmaputra River, the Meghna River and the Indus River. The results reveal that the Atrai River sediments are texturally immature and subarkose types, while almost all of the Himalayan rivers sediments are dominated by moderate textural maturity and arkose to litharenites in nature (Bhuiyan et al. 2011; Hossain 2019; Huyan et al. 2021; Singh 2010). Based on weathering indices (CIA, PIA, and CIW), low to moderate chemical weathering is consistent for all the southern Himalayan river. The CIA values of the Atrai River sediments varies from 54.11 to 58.91 with an average value of 55.00, which is very close to the CIA values of the Brahmaputra River (ranges from 51 to 62 with averages of 53) (Bhuiyan et al. 2011) and Ganges River (ranges from 47.9 to 54.7) (Singh 2010). A low-to-moderate chemical weathering intensity is also suggested by Hossain (2019) for the Meghna River (CIA value ranges from 55 to 69) and Huyan et al. (2021) for the Yarlung Zangbo (upper reaches of the Brahmaputra) River (CIA value ranges from 49 to 70) sediments. In addition, very low CIA values (ranges from 48 to 52) were reflected in Indus River sediment (Ahmed et al. 1998).

The provenance discriminant diagram of F1-F2 (Roser and Korsch 1988) reveals that the Atrai River sediments fall within the felsic igneous sources (Fig. 8a), while the Brahmaputra and Meghna River sediments fall in the quartzose recycled field (Bhuiyan et al. 2011; Hossain 2019). The Yarlung Zangbo River sediments, on the other hand, are scattered both in the felsic igneous and quartzose fields (Huyan et al. 2021). Overall, the Atrai River sediments suggest an active margin tectonic setting (Fig. 13a–d), which is consistent with the Brahmaputra River sediments, although there is some difference in the Yarlung Zangbo River with partial affinity with the continental island arc and in the Meghna River with the transition from active to passive margin settings.

Conclusion

This research supports the following conclusions:

a. The Atrai River sediments are medium-grained, moderately well sorted, and composed of quartz (Qm), feldspar, micas, and rock fragments. The average modal composition ($Q_{77.13}F_{16.01}L_{6.86}$) classified them as sub-arkose, which is also in accordance with the geochemical result.
b. Petrographic and geochemical signatures indicate that the investigated sediments are compositionally immature.
c. The geochemical and petrographic provenance discrimination diagrams and geochemical ratios suggest a dominating granitic suite of felsic igneous provenance for the Atrai River sediments, and they were mainly derived from the Higher Himalayan Crystalline Series as well as the Lesser Himalayan crystalline rocks.
d. The weathering indices (CIA, CIW, PIA, and ICV) and collective chemical compositions of the Atrai River sediments reflect a low-to-moderate intensity of chemical weathering in the southeast Himalaya.
e. The tectonic discriminate diagrams point to an active margin tectonic setting for the Atrai River sediments.

Acknowledgements The authors are also grateful to the Institute of Mining, Mineralogy and Metallurgy (IMMM), BCSIR, for allowing us in their XRF laboratory. A special thanks goes to Mr. Masum Shah for his kind cooperation during the field work.

Funding This work is funded by the Faculty of Physical and Mathematical Sciences, Jahangirnagar University.

Data Availability The authors confirm that the data supporting the findings of this study are available within the article.

Declarations

Conflict of interest The authors declare that they no competing interests.

References

Abdullah R, Aurthy MR, Khanam F, Hossain M, ASM S (2022) Structural development and tectonostratigraphic evolution of the Sylhet Trough (northeastern Bengal Basin) in the context of Cenozoic Himalayan Orogeny: Insights from geophysical data interpretation. Mar Pet Geol 138:105544

Abdullah R, Sayem ASM, Yeasmin R, Rahman MM, Bari Z, Khanam F (2021) Plio-Pleistocene to Recent Tectonostratigraphic evolution of the Lalmai Anticline in the western Indo-Burman Range (Bangladesh): insights from lithofacies analysis and structural synthesis. Arab J Geosci 14:392

Abeden MJ, Rahman MJJ, Sayem ASM, Abdullah R (2017) Heavy mineral distribution in sand deposits from the lower reaches of the Jamuna River, Bangladesh. Bangladesh Geosci J 24:1–14

Ahmed T, Khanna PP, Chakranpani GJ, Balakrishnan S (1998) Geochemical characteristics of wate and sediment of the Indus River, Trans-Himalaya, India: constrians on weathering and eroison. J Asian Earth Sci 16:333–346

Al-Dousari A, Doronzo D, Ahmed M (2017) Types, indications and impact evaluation of sand and dust storms trajectories in the Arabian gulf. Sustainability 9:1526

Al-Hemoud A, Al-Dashti H, Al-Saleh A et al (2022) Dust storm 'hot spots' and transport pathways affecting the Arabian Peninsula. J Atmos Sol Terr Phys 238-239:105932

Armstrong-Altrin J, Verma SP (2005) Critical evaluation of six tectonic setting discrimination diagrams using geochemical data of Neogene sediments from known tectonic setting. Sediment Geol 177:115–129

Armstrong-Altrin JS, Lee YI, Kasper-Zubillaga JJ, Trejo-Ramírez E (2017) Mineralogy and geochemistry of sands along the Manzanillo and El Carrizal beach areas, southern Mexico: implications for palaeoweathering, provenance, and tectonic setting. Geol J 52:559–582

Armstrong-Altrin JS, Machain-Castillo ML, Rosales-Hoz L, Carranza-Edwards A, Sanchez-Cabeza J, Ruíz-Fern Andez AC (2015) Geochemistry of deep sea sediments from the south-western Gulf of Mexico, Mexico: implication for depositional environment. Cont Shelf Res 95:15–26

Armstrong-Altrin JS, Madhavaraju J, Vega-Bautista F, Ramos-Vazquez MA, Perez-Alvarado BY, Kasper-Zubillaga JJ, AZE B (2021) Mineralogy and geochemistry of Tecolutla and Coatzacoalcos beach sediments SW Gulf of Mexico. Appl Geochem 134:105103

Armstrong-Altrin JS, Nagarajan R, Madhavaraju J, Rosalez-Hoz L, Lee YI, Balaram V, Cruz-Martinez A, Avila-Ramirez G (2013) Geochemistry of the Jurassic and upper Cretaceous shales from the Molango Region, Hidalgo, Eastern Mexico: implications of source-area weathering, provenance, and tectonic setting. Geoscience 345:185–202

Bayon G, Toucanne S, Skonieczny C, André L, Bermell S, Cheron S et al (2015) Rare earth elements and neodymium isotopes in world river sediments revisited. Geochim Cosmochim Acta 170:17–38

Bhatia MR (1983) Plate tectonics and geochemical composition of sandstones. J Geol 91:611–627

Bhuiyan MAH, Rahman MJJ, Dampare SB, Suzuki S (2011) Provenance, tectonics and source weathering of modern fluvial sediments of the Brahmaputra–Jamuna River, Bangladesh: Inference from geochemistry. J Geochem Explor 111:113–137

Condie KC (1967) Geochemistry of early Precambrian greywackes from Wyoming. Geochim Comochim Acta 31:2135–2149

Condie KC, Noll PD, Conway CM (1992) Geochemical and detrital mode evidence for two sources of Early Proterozoic metasedimentary rocks from the Tonto Basin upergroup, central Arizona. Sediment Geol 77:51–76

Cox R, Lowe DR, Cullers RL (1995) The influence of sediment recycling andbasement composition on evolution of mudrock chemistry in the southwestern United States. Geochim Cosmochim Acta 59:2919–2940

Critelli S, Ingersoll RV (1994) Sandstone petrology and provenance of the Siwalik Group (northwestern Pakistan and western-southeastern Nepal). J Sediment Res 64:815–823

Cullers RL (1995) The controls on the major and trace element evolution of shales, siltstones and sandstones of Ordovician to Tertiary age in the Wet Mountain region, Colorado, U.S.A. Chem Geol 123:107–131

Cullers RL (2000) The geochemistry of shales, siltstones and sandstones of Pennsylvanian-Permian age, Colorado, USA: implications for provenance and metamorphic studies. Lithos 51:181–203

Dasgupta S, Ganguly J, Neogi S (2004) Inverted metamorphic sequence in the Sikkim Himalayas: crystallization history, P-T gradient, and implications. J Metamorph Geol 22:395–412

Dickinson WR (1985) Interpreting provenance relations from detrital modes of sandstone. In: Zuffa (ed) Provenance of arenites. Advanced Study Institute Series, D. Reidel Publishing Company, Dordrecht, The Netherlands

Dickinson WR, Beard LS, Brakenridge GR, Erjavec JL, Ferguson RC, Inman KF, Knepp RA, Lindberg FA, Ryber PT (1983) Provenance of North American Phanerozoic sandstones in relation to tectonic setting. Geol Soc Am Bull 94:222–235

Dickinson WR, Suczek CA (1979) Plate tectonics and sandstone compositions. AAPG Bull 63:2164–2182

Doronzo DM (2012) Two new end members of pyroclastic density currents: forced convection-dominated and inertia-dominated. J Volcanol Geotherm Res 219:87–91

Fedo CM, Nesbitt HW, Young GM (1995) Unraveling the efects of potassium metasomatism in sedimentary rocks and paleosols, with implications for paleoweathering conditions and provenance. Geology 23:21–924

Folk RL, Ward WC (1957) Brazos River bar, a study in the significance of grain size parameters. J Sediment Petrol 27:3–26

Galy A, France-Lenord C (2001) Higher erosion rates in the Himalaya: geochemical constrains on riverine fluxes. Geology 29:23–26

Garver JI, Royce PR, Smick TA (1996) Chromium and nickel in shale of the Taconic Foreland: a case study for the provenance of fiegrained sediments with an ultramafic source. J Sediment Res 66:100–106

Goto A, Tatsumi Y (1994) Quantitative analysis of rock samples by an X-ray fluorescence spectrometer (I). The Rigaku Journal 11:40–59

Goto A, Tatsumi Y (1996) Quantitative analysis of rock samples by an X-ray fluorescence spectrometer (II) [J]. Rigaku J 13:20–38

Harnois L (1988) The CIW index: a new chemical index of weathering. Sediment Geol 55:319–322

Hayashi K, Fujisawa H, Holland HD, Ohmoto H (1997) Geochemistry of 1.9 Ga sdimentary rocks from northeastern Labrador Canada. Geochim Cosmochim Acta 61:4115–4137

He Z, Guo ZT, Yang F, Sayem ASM, Wu H, Zhang Z, Hao Q, Xiao G, Han L, Fu Y, Wu Z, Hu H (2019) Provenance of Cenozoic sediments in the Xining Basin revealed by Nd and Pb isotopic evidence: implications for tectonic uplift of the NE Tibetan Plateau. Geochem Geophys Geosyst 20:4531–4544

Herron MM (1988) Geochemical classification of terrigenous sands and shales from core or log data. J Sediment Petrol 58:820–829

Hossain HMZ (2019) Major, trace, and REE geochemistry of the Meghna River sediments, Bangladesh: constraints on weathering and provenance. Geol J 55:3321–3343

Huyan Y, Yao W, Wang L (2021) Provenance, source weathering, and tectonics of the Yarlung Zangbo River overbank sediments in Tibetan Plateau, China using major, trace, and rare earth elements. Geol J 57:37–51

Jacobson AD, Blum JD, Chamberlain CP, Craw D, Koons PO (2003) Climatic and tectonic controls on chemical weathering in the New Zealand Southern Alps. Geochim Cosmochim Acta 67:29–46

Kundu A, Matin A, Eriksson PG (2016) Petrography and geochemistry of the Middle Siwalik sandstones (tertiary) in understanding the provenance of sub-Himalayan sediments in the Lish River Valley, West Bengal India. Arab J Geosci 9:162

Le Bas MJ, Le Maitre RW, Streckeisen A, Zanettin B (1986) A chemical classification of volcanic rocks based on the total alkali–silica diagram. J Petrol 27:745–750

Li L, Ni J, Chang F, Yue Y, Frolova N, Magritsky D et al (2020) Global trends in water and sediment fluxes of the world's large rivers. Sci Bull 65:62–69

Long X, Yuan C, Sun M, Xiao W, Wang Y, Cai K, Jiang Y (2012) Geochemistry and Nd isotopic composition of the Early Paleozoic flysch sequence in the Chinese Altai, Central Asia: evidence for a northward-derived mafic source and insight into model ages in an accretionary orogen. Gondwana Res 22:554–566

Mange MA, Maurer HFW (1992) Heavy minerals in color. Chapman and Hal, London, p 133

McLennan SM (1989) Rare earth elements in sedimentary rocks: influence of provenance and sedimentary processes. Rev Mineral 21:169–200

McLennan SM, Hemming S, McDaniel DK, Hanson GN (1993) Geochemical approaches to sedimentation, provenance, and tectonics. In: Basu, A., Johnsson, M.J. (Eds.), Processes controlling the composition of clastic sediments. Geol Soc Am Spec Pap 284:21–40

Najman Y, Bickle M, BouDagher-Fadel MK et al (2008) The Paleogene record of Himalayan erosion: Bengal Basin, Bangladesh. Earth Planet Sci Lett 273:1–14

Nesbitt HW, Young GM (1982) Early Proterozoic climates and plate motions inferred from major element chemistry of lutites. Nature 299:715–717

Nesbitt HW, Young GM (1984) Prediction of some weathering trends of plutonic and volcanic rocks based on thermodynamic and kinetic considerations. Geochim Cosmochim Acta 48:1523–1534

Noa Tang SD, Ntsama Atangana J, Onana VL (2020) Mineralogy and geochemistry of alluvial sediments from the Kadey plain, eastern Cameroon: implications for provenance, weathering, and tectonic setting. J Afr Earth Sci 163:103763

Parker A (1970) An index of weathering for silicate rocks. Geol Mag 107:501–504

Pettijohn FJ, Potter PE, Siever R (1972) Sand and sandstone. Plate motions inferred from major element chemistry of lutites. Precambrian Res 147:124–147

Potter PE (1978) Petrology and chemistry of modern big river sands. J Geol 86:423–449

Rahman MJJ, Sayem ASM, Bhuiyan MH (2014a) Geochemistry of the Plio–Pleistocene Dupi Tila sandstones from the Surma Basin, Bangladesh: implications for provenance, tectonic setting and weathering. Himal Geol 35:162–170

Rahman MJJ, Sayem ASM, McCann T (2014b) Geochemistry and provenance of the Miocene Sandstones of the Surma Group from the Sitapahar Anticline, southeastern Bengal Basin, Bangladesh. J Geol Soc India 83:447–456

Rahman MJJ, Xiao W, Hossain MS, Yesmin R, Sayem ASM, Ao S, Yang L, Abdullah R, Dina NT (2020) Geochemistry and detrital zircon U-Pb dating of Pliocene-Pleistocene sandstones of the Chittagong Tripura Fold Belt (Bangladesh): implications for provenance. Gondwana Res 78:278–290

Rahman MM, Arya DS, Goel NK, Dhamy AP (2011) Design fow and stage computations in the Teesta River, Bangladesh, using frequency analysis and MIKE 11 modeling. J Hydrol Eng 16:176–186

Ranjan N, Bannerjee DM (2009) Central Himalayan crystallines as the primary source for the sandstone–mudstone suites of the Siwalik Group: new geochemical evidence. Gondwana Res 6:687–696

Rosales-Lagarde L, Centeno-García E, Dostal J, Sour-Tovar F, Ochoa-Camarillo H, Quiroz-Barroso S (2005) The Tuzancoa Formation: evidence of an Early Permian submarine continental Arc in East-Central Mexico. Int Geol Rev 47:901–919

Roser BP, Korsch RJ (1986) Determination of tectonic setting of sandstone-mudstone suites using SiO_2 content and K_2O/Na_2O ratio. J Geol 94:635–650

Roser BP, Korsch RJ (1988) Provenance signatures of sandstone-mudstone suites determined using discrimination function analysis of major element data. Chem Geol 67:119–139

Roser BP, Cooper RA, Nathan SA, Tulloch AJ (1996) Reconnaissance sandstone geochemistry, provenance, and tectonic setting of the lower Paleozoic terrains of the West Coast and Nelson, New Zealand. N Z J Geol Geophys 39:1–16

Ruddiman WF (2008) Earth's climate: past, present and future. WH Freeman and Company, New York, p 387

Sayem ASM, Guo ZT, Wu H, Zhang C, Yang F, Xiao G, He Z (2018) Sedientary and geochemical evidence of Eocene climate change in the Xining Basin, northeastern Tibetan Plateau. Sci China Earth Sci 61:1292–1305

Sayem ASM, Shoshi KF, Rokonuzzaman M, Abeden MJ, Bari Z (2021) Textural and heavy mineral characteristics of the bar sediments from the upper reaches of the Atrai River, northwest Bangladesh. Bangladesh Geosci J 27:17–41

Singh P (2010) Geochemistry and provenance of stream sediments of the Ganga River and its major tributaries in the Himalayan region India. Chem Geol 269:220–236

Suttner LJ, Dutta PK (1986) Alluvial sandstone composition and paleoclimate framework mineralogy. J Sediment Petrol 56:329–345

Taylor SR, McLennan SM (1985) The continental crust: its composition and evolution. an examination of the geochemical record preserved in sedimentary rocks. Blackwell Science, Oxford

Torres-Sanchez D, Verma SK, Verma SP, Velasco-Tapia F, Torres-Hernandez JR (2019) Petrogenetic and tectonic implications of Oligocene-Miocene volcanic rocks from the Sierra de San Miguelito complex, central Mexico. J S Am Earth Sci 95:102311

Uddin A, Lundberg N (1998) Unroofing history of the eastern Himalaya and the Indo–Burman ranges: heavy mineral study of Cenozoic sediments from the Bengal Basin, Bangladesh. J Sediment Res 68:465–472

Verma SP (2015) Origin, evolution, and tectonic setting of the eastern part of the Mexican Volcanic Belt and comparison with the Central American Volcanic Arc from conventional multielement normalized and new multidimensional discrimination. Turk J Earth Sci 24:111–164

Verma SP, Armstrong-Altrin JS (2013) New multi-dimensional diagrams for tectonic discrimination of siliciclastic sediments and their application to Precambrian basins. Chem Geol 355:117–180

Viers J, Dupré B, Gaillardet J (2009) Chemical composition of suspended sediments in World Rivers: new insights from a new database. Sci Total Environ 407:853–868

Wentworth CK (1922) A scale of grade and class terms for clastic sediments. J Geol 30:377–392

Wronkiewicz DJ, Condie KC (1987) Geochemistry of Archean shales from the Witwatersrand Supergroup, South Africa: source-area weathering and provenance. Geochim Cosmochim Acta 51:2401–2416

Wronkiewicz DJ, Condie KC (1990) Geochemistry and mineralogy of sediments from the Ventersdorp and Transvaal Supergroups, South Africa: Cratonic evolution during the early Proterozoic. Geochim Cosmochim Acta 54:343–354

Yang L, Xiao WJ, Rahman MJJ et al (2020) Indo-Burma passive amalgamation along the Kaladan Fault: insights from zircon provenance in the Chittagong-Tripura Fold Belt (Bangladesh). GSA Bull 132:1953–1968

Zaid SM (2015) Geochemistry of sandstones from the Pliocene Gabir Formation, north Marsha Alam, Red sea, Egypt: implication for provenance, weathering and tectonic setting. J Afr Earth Sci 102:1–17